



Research paper

Ultrafast photo-induced charge transfer of 1-naphthol and 2-naphthol to halocarbon solvents



Subhajyoti Chaudhuri^{a,b}, Benjamin Rudsteyn^b, Mirabelle Prémont-Schwarz^c, Dina Pines^d, Ehud Pines^d, Dan Huppert^e, Erik T.J. Nibbering^{c,*}, Victor S. Batista^{b,*}

^a School of Engineering and Applied Science, 10 Hillhouse Ave, Yale University, New Haven, CT 06520, USA

^b Department of Chemistry, P.O. Box 208107, Yale University, New Haven, CT 06520, USA

^c Max Born Institut für Nichtlineare Optik und Kurzzeitspektroskopie, Max Born Strasse 2A, 12489 Berlin, Germany

^d Department of Chemistry, Ben Gurion University of the Negev, P.O.B. 653, Beersheva 84105, Israel

^e Raymond and Beverly Sackler Faculty of Exact Sciences, School of Chemistry, Tel Aviv University, Tel Aviv 69978, Israel

ARTICLE INFO

Article history:

Received 9 January 2017

In final form 28 March 2017

Available online 29 March 2017

Keywords:

Naphthols

Ultrafast spectroscopy

Photo-induced charge transfer

Electron donor acceptor interactions

DFT

Marcus theory

ABSTRACT

We explore the fluorescence quenching of 1-naphthol and 2-naphthol in halocarbon solvents by using time-correlated single-photon-counting, femtosecond IR-spectroscopy and quantum chemistry computations. We find that halocarbon solvents facilitate a de-excitation mechanism via solute-solvent electron transfer. Decay rates are modulated by close contact interactions between the π -electronic structure of naphthols and halocarbon molecules in their first solvation shell. 1-naphthol exhibits faster decay rates than 2-naphthol due to closer interactions with the solvent.

© 2017 Published by Elsevier B.V.

1. Introduction

Photo-induced electron transfer (ET) in donor-acceptor reaction pairs has been a topic of intense research for decades [1,2]. With the technological advance of femtosecond lasers, it has become possible to follow the elementary steps of electron transfer. Resolving the underlying microscopic mechanisms and elucidating transient structures has been a major goal in the field of femtochemistry [3]. Photochemical events initiated in molecular clusters have provided fundamental insights on donor-acceptor interactions in the gas phase [4]. Specially designed donor-acceptor systems in molecular assemblies, including DNA, provided an appealing route to resolve photoinduced molecular mechanisms [5]. Solution phase systems have been more challenging to tackle due to their inherent complexities. Intrinsic donor-acceptor reaction dynamics [6] is often found to be ultrafast (sub-picosecond to several picoseconds) and intertwined with the much

slower molecular diffusion dynamics (from sub-nanosecond time scales and longer). Nevertheless, the ultrafast electron transfer between donor and acceptor molecules can still be characterized in a polar solution by steering the outcome of the reaction according to the Marcus relationship. Often a solvent actively participates in photo-induced electron transfer, acting either as donor or acceptor. Here, the role of mutual diffusion of reactants is diminished to mere local reorganization [7–10]. In this paper, we address the effect of specific solvent-solute interactions that modulate the rate of the relaxation mechanism.

Ultrafast electronic and vibrational pump-probe spectroscopy has been utilized to characterize the photo-induced charge transfer dynamics of a large variety of molecular donor-acceptor systems. Such studies reveal many aspects of the excited states involved in the forward charge transfer reaction dynamics [11–14], provide structural information of transient states, [15–17] and characterize the quantum yields of photo-products and possible ground-state recovery by charge back-transfer [18]. Often these donor or acceptor molecules are molecular systems with aromatic π -molecular orbitals, which play a major role in the donor-acceptor interactions. This is also often the case for aromatic molecular systems with additional molecular functionalities, e.g. an OH group, as found in photoacid molecular systems. Photoacid molecules have

Abbreviations: DFT, density functional theory; TD-DFT, time dependent density functional; ET, electron transfer.

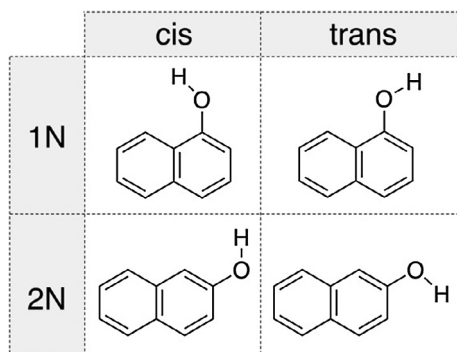
* Corresponding authors.

E-mail addresses: nibberin@mbi-berlin.de (E.T.J. Nibbering), victor.batista@yale.edu (V.S. Batista).

been utilized to probe photoinduced proton transfer dynamics, mostly in studies of the ultrafast spectroscopy of photoacid-base neutralization [19–24].

The molecular mechanisms responsible for photoacidity remain controversial and a subject of current debate [23]. In contrast to conventional pictures where optical excitation leads to (partial) charge transfer away from the electronegative atom in the proton-donating group, state-of-the-art quantum chemical calculations have indicated that the net charge flow in the photoacid is rather minor [25,26]. Instead, the driving force for photoacidity is thought to be due to the much larger charge density changes in the conjugated photobase side of the Förster cycle [25,26]. One local probe of the hydrogen bond is the O–H stretching mode. The O–H stretching frequency typically shows a direct correlation with the hydrogen bond strength (i.e., red-shifted for stronger hydrogen bonds) although specific solute-solvent interactions might also affect the frequency shifts. A combined experimental and theoretical study has recently shown that the O–H stretching mode frequency can be correlated to photoacidity, as determined by the hydrogen bond structure in terms of O...N or O–H distances, for complexes of 2-naphthol and other aromatic alcohols hydrogen-bonded with acetonitrile. Interestingly, it was shown that photoexcitation of 2-naphthol did not induce significant changes in the distribution of atomic charges in the OH group [27], supporting the notion that photoacidity is not so much determined by photoinduced changes in the photoacid side but rather on the conjugated photobase. A question arises whether charge flow in photoacid molecules in photoinduced proton transfer dynamics can be correlated to charge flow when these photoacid molecules function as photoinduced electron donor systems.

Here, we investigate the excited-state dynamics of 1-naphthol (1N) and 2-naphthol (2N) in halocarbon solvents such as CCl_4 , C_2Cl_4 , and CHCl_3 (Scheme 1) to explore specific interactions and changes of charge distributions induced by 1N and 2N photoexcitation. The solvents CCl_4 , C_2Cl_4 , and CHCl_3 induce major fluorescence quenching [28–33], suggesting charge transfer solute-solvent interactions. We explore the dynamical processes that determine the excited-state lifetimes of 1N and 2N by using time-correlated single-photon counting (TCSPC) measurements of the fluorescence emission, as well as femtosecond IR spectroscopic measurements to probe the dynamics through potentially dark states as well as possible ground-state recovery. We observe a major electronic excited state lifetime shortening for CCl_4 , and to some extent C_2Cl_4 , whereas for CHCl_3 the effect is smaller. We perform quantum-chemical calculations of the S_0 - and S_1 -states of 1N and 2N in CCl_4 to elucidate the underlying molecular mechanisms of photo-induced charge transfer in halocarbon solvents. We assess whether these solute-solvent interactions provide insights on changes of charge distributions caused by photoexcitation. We determine the relative energetics of different conformations



Scheme 1. 1-naphthol (1N) and 2-naphthol (2N) in either *cis* or *trans* configurations.

[34,35] due to the rotational degree of freedom of the hydroxyl-group of 1N and 2N embedded in halocarbon solvents. We calculate *ab initio* electron transfer rates at the density functional theory level, using a Bixon-Jortner approach within the framework of Marcus Theory [36], and compare the relative decay rates for 1N and 2N as determined by specific interactions with halocarbon molecules in their first solvation shells.

2. Details on experiments

2.1. Samples, solvents, steady-state and time-resolved measurements

1-naphthol (1N), and 2-naphthol (2N) were purchased from Sigma-Aldrich and used as delivered. The solvents cyclohexane, CCl_4 , C_2Cl_4 , and CHCl_3 and acetonitrile (Sigma-Aldrich) were dried over molecular sieves. CDCl_3 was obtained from Deutero GmbH and used without further purification. Care was taken that halogenated solvents contained only aprotic, if any, stabilizers. Electronic absorption and fluorescence spectra have been recorded with a Perkin-Elmer UV-vis spectrometer and a JOBIN YVON Horiba fluorolog, respectively. Steady-state FT-IR spectra were recorded with a Varian 640 FT-IR spectrometer. Time-correlated single photon counting (TCSPC) signals have been detected using a Hamamatsu 3809U MCP photomultiplier and an Edinburgh Instruments TCC 900 integrated TCSPC system. The time response of the instrument was approximately 40 ps FWHM. Excitation occurred with pump pulses centered at 265 or 293 nm using the triple harmonic of a cavity-dumped Ti-sapphire femtosecond laser (Mira; Coherent) [37]. Ultrafast UV-pump mid-IR-probe measurements on 1N and 2N were performed as described in detail previously [38,39]. Typically excitation pulses centered at 318 to 330 nm, with 50 fs duration and $\sim 3 \mu\text{J}$ energies were used to promote 1N or 2N to the S_1 -state (1L_b -state). Effective time resolution in ultrafast UV-pump IR-probe experiments was typically 150–200 fs due to group velocity mismatch between pump and probe pulses, when propagating through 300 μm thick flow cells.

3. Experimental results

Fig. 1 shows the absorption and fluorescence spectra of 1N and of 2N in cyclohexane as well as in the halocarbon solvents. We observe a major fluorescence quenching effect with fluorescence quantum yields decreasing in the order $\text{CHCl}_3 > \text{C}_2\text{Cl}_4 > \text{CCl}_4$, much akin to previously reported quenching of naphthalene and other aromatic compounds in these solvents [29–33].

Fig. 2 shows the TCSPC measurements of 1N and 2N dissolved in CCl_4 , C_2Cl_4 and CHCl_3 as well as in cyclohexane. We note the increase in the fluorescence decay rate when going from cyclohexane, via CHCl_3 , C_2Cl_4 and CCl_4 . Moreover, faster decay rates are observed for 1N than for 2N. Noting that the fluorescence decay of 1N and 2N in cyclohexane (lifetimes have been measured to be 4.7 ns and 4.6 ns, respectively) indicates a predominantly electronic excited state decay by radiative emission, the substantial lifetime shortening of 1N and 2N in the halocarbon solvents strongly hint at the key role(s) of different de-excitation mechanism(s). Furthermore, we observe fluorescence decay dynamics on multiple time scales, suggesting that different fractions of the naphthol chromophores undergo these de-excitation processes through different pathways. Multiple exponential fitting has been applied to provide a first characterization of the fluorescence decay times. The resulting fitting parameters are summarized in Table 1. We note that the fluorescence decay times measured for both 1N and 2N in CCl_4 have major components close to (or even shorter than) the instrument response time, making it impossible to obtain reliable fluorescence decay times for 2N and in particular, 1N in CCl_4 .

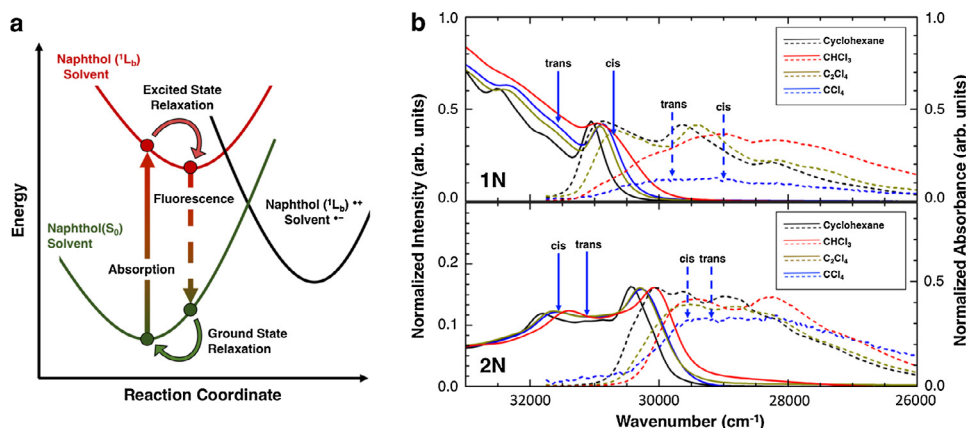


Fig. 1. (a) Schematic diagram showing excited and ground state structural relaxations as the origin of the red-shift in fluorescence. (b) Absorption (solid lines) and fluorescence (dashed lines) spectra of the $S_0 \rightarrow {}^1L_b$ (S_1) electronic transition of 1N and 2N measured in cyclohexane, CCl_4 , C_2Cl_4 and $CDCl_3$ solution. Computed positions for absorption and fluorescence of the relevant electronic transition for *cis* and *trans* isomers have been indicated with solid and dashed arrows respectively. (For interpretation of the references to colour in this figure legend, the reader is referred to the web version of this article.)

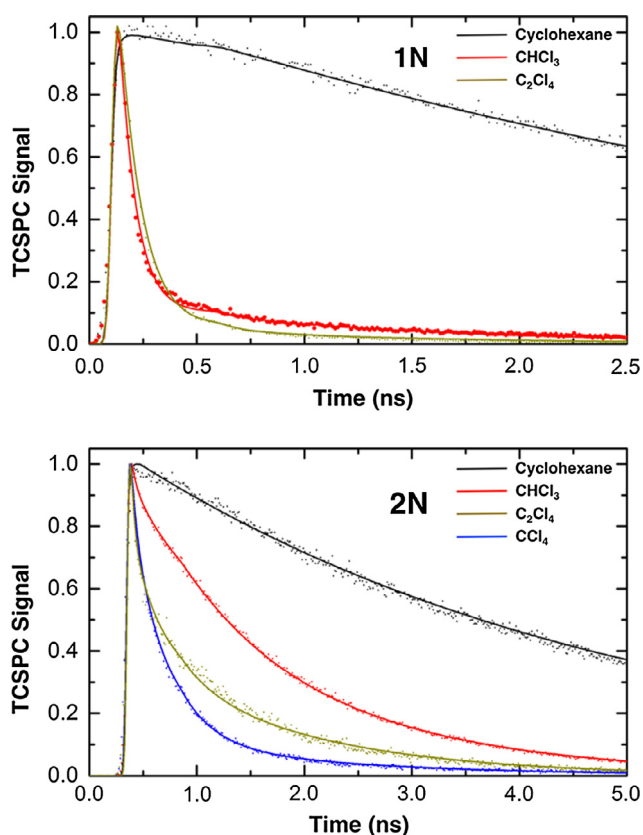


Fig. 2. TCSPC measurements of 1N (top) and 2N (bottom) measured in cyclohexane, CCl_4 , C_2Cl_4 and $CHCl_3$ solution. Multiexponential fits are shown as solid lines (see Table 1 for fitting results). No attempt was made to fit the TCSPC signal of 1N in CCl_4 , because its decay has major components shorter than the instrument response time.

To obtain more insight into the characteristics of the quenching mechanism we have utilized femtosecond UV-pump/IR-probe spectroscopy. Here, one has in principle the option to detect not only IR-active marker modes of the initially excited 1L_b -state of 1N and 2N, as well as determine possible quantum yields of the S_0 -state recovery at ultrafast time scales, but may also detect IR-active marker modes of possible intermediate dark states, initially reached after the photo-excited 1N or 2N S_1 -state relaxes. Fig. 3 shows the transient IR spectra recorded for 1N in CCl_4 , C_2Cl_4 and

$CDCl_3$, both in the fingerprint region and in the O–H stretching region. We have focused our attention to the $1200\text{--}1300\text{ cm}^{-1}$ spectral range, as this spectral range has the right transparency conditions for all solvents used, together with the occurrence of strong marker bands for both 1N and 2N in both electronic ground and excited states.

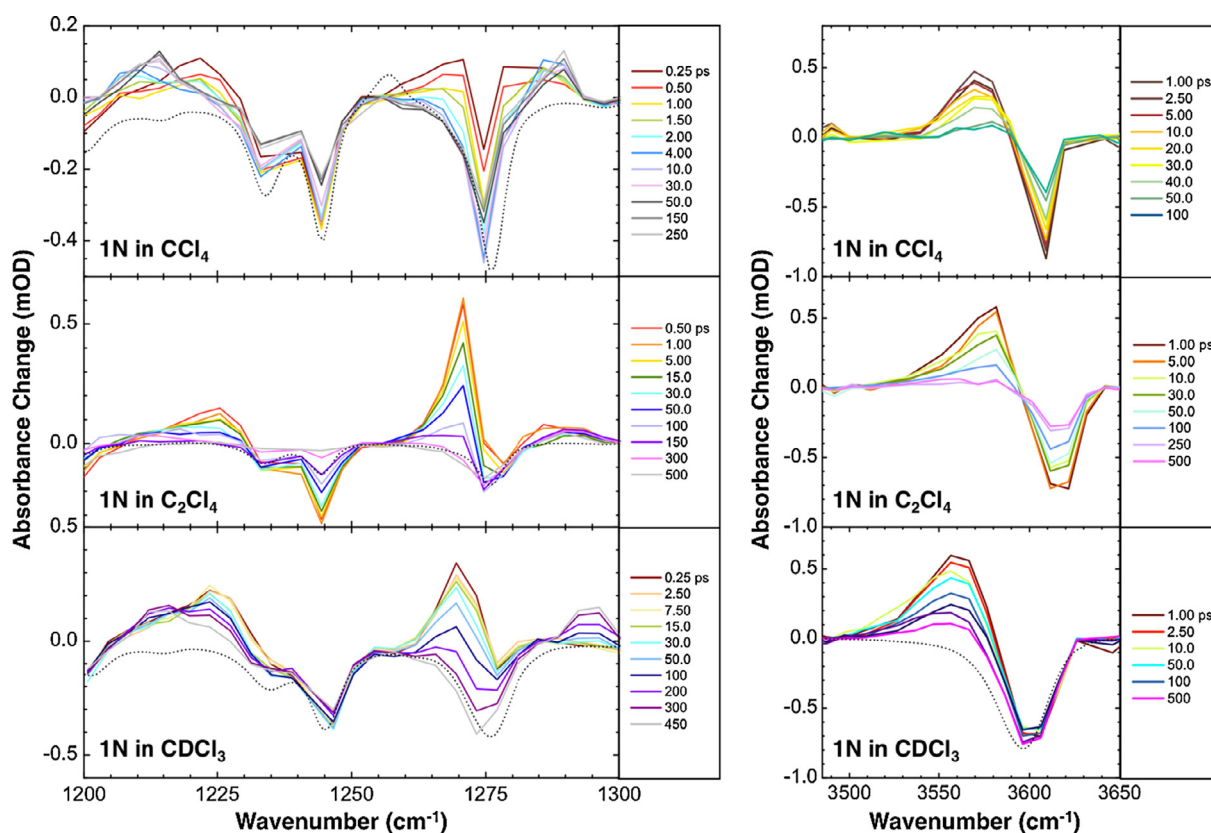
We observe bleach signals at positions where 1N has its fingerprint transitions and O–H stretching transitions in the S_0 -state. Positive absorbance signals appearing within time resolution are located at 1221 , 1226 and 1271 cm^{-1} in the fingerprint region for all solvents CCl_4 , C_2Cl_4 and $CDCl_3$ (albeit with different spectral broadening, and a marked spectral blue-shifting indicative of vibrational cooling for CCl_4 only, see e.g. the band at 1285 cm^{-1}), and at 3570 , 3581 and 3560 cm^{-1} for the O–H stretching mode of 1N in CCl_4 , C_2Cl_4 and $CDCl_3$, respectively. These transitions are indicative of IR-active modes in the S_1 -state. A frequency downshift of the O–H stretching mode upon electronic excitation to the 1L_b -state has been previously reported, including the role of the dielectric solvent medium on the frequency shifts [34,35]. These signals decay at particular solvent-dependent time scales, and are accompanied by a partial bleach recovery, ranging from $60 \pm 10\%$ in CCl_4 within 50 ps, $60 \pm 10\%$ in C_2Cl_4 within 200 ps, and no significant ground-state recovery in $CDCl_3$ within 1 ns, the maximum value of our delay stage. This observation for C_2Cl_4 and, in particular CCl_4 as solvent hints at electronic excited state decay pathways facilitating an efficient electronic ground state recovery. Positive signals persisting to delay times up to 1 ns are understood to be spectral signatures of transient states reached upon S_1 -decay for that fraction of initially excited molecules not following a fast pathway to ground state recovery. Marker bands for this transient species reached after initial decay of the S_1 -state are observed at $1214\text{--}1216$, $1266\text{--}1270$ and $1290\text{--}1296\text{ cm}^{-1}$. We did not pursue a particular spectral characterization of these transient states. We note in concluding here that besides observing the O–H stretching bands of 1N and of 2N in the S_1 -state, and its associated bleach signal located at the O–H stretching band of the S_0 -state, we have not been able to identify a transient IR-signature of the O–H stretching mode indicative of the intermediate state reached after decay of the S_1 state.

We recorded similar results for 2N in CCl_4 , C_2Cl_4 , and $CDCl_3$ (data not shown here, see also earlier published data) [38]. While 2N has a different IR-active fingerprint pattern in electronic ground and excited states when comparing to those of 1N, the general dynamical features are similar, albeit significantly slower.

Table 1

Multi-exponential fitting parameter values obtained with TCSPC and UV-IR measurements for 1N and 2N in halocarbon solvents.

Chromophore	Solvent	TCSPC ^a	UV-IR ^b	
			S ₁ decay	S ₀ recovery
1N	CCl ₄	–	1.4 ps	1.4 ps (0.5) >1 ns ^c (0.5)
	C ₂ Cl ₄	100 ps (0.96)	60 ps (0.85)	60 ps (0.6)
	CHCl ₃ /CDCl ₃ ^d	70 ps (0.92)	50 ps (0.25)	>1 ns ^c (0.5)
		1.5 ns (0.08)	400 ps (0.75)	–
2N	CCl ₄	<30 ps (0.45)	13 ps	13 ps (0.4)
		200 ps (0.30)		>1 ns ^c (0.6)
		1.5 ns (0.25)		
	C ₂ Cl ₄	<40 ps (0.30)	150 ps (0.3)	150 ps (0.5)
		300 ps (0.51)	1 ns (0.7)	1 ns (0.5)
		1.5 ns (0.09)		
	CHCl ₃ /CDCl ₃ ^d	<40 ps (0.20)	>50 ps	>50 ps
		900 ps (0.40)		
		1.9 ns (0.40)		

^a Detection wavelength: 355 nm.^b Derived from fitting the O–H stretching marker bands in the S₁-state and S₀-states.^c Long time component extending significantly beyond scanning range.^d TCSPC measurements were performed with CHCl₃, UV-IR measurements were performed with CDCl₃.**Fig. 3.** Transient UV-pump/IR-probe spectra of 1N and 2N measured in CCl₄, C₂Cl₄ and CHCl₃ solution. These transient IR spectra have been recorded for the 1200–1300 cm⁻¹ fingerprint and in the O–H stretching spectral ranges. Steady-state IR spectra of 1N in the S₀-state are shown as inverted short-dashed traces.

We now refer to Fig. 4, showing the kinetics upon excitation of the S₀ → S₁ electronic transition, as derived from the O–H stretching marker mode. Similar kinetics can be observed when probing the IR-active fingerprint transitions, where a clear analysis is hampered by the substantial spectral overlap with ground state bleach signals, and possible vibrational cooling effects. From the O–H stretching marker mode probed in S₁-state, and comparing this with the kinetics of the ground state bleach signals, we learn that the decay kinetics of the S₁-state matches the bleach recovery kinetics, albeit that the S₁-decay is dominated by fast components

for all members of the ensemble (although a long-time component with small magnitude is suggested by the experimental data), whereas the bleach recovery is only partial. Exponential fitting provides a characterization of the relevant time scales much alike from those obtained from the TCSPC measurements. The ratio of steady-state fluorescence intensities $Y_F(\text{halocarbon})/Y_F(\text{cyclohexane})$ observed for 1N and 2N in the halocarbon solvents compared to those recorded for cyclohexane turn out to be similar to the ratio in fluorescence decay times (using the time constant of the major component), or the O–H stretching band decay of the S₁-state. For

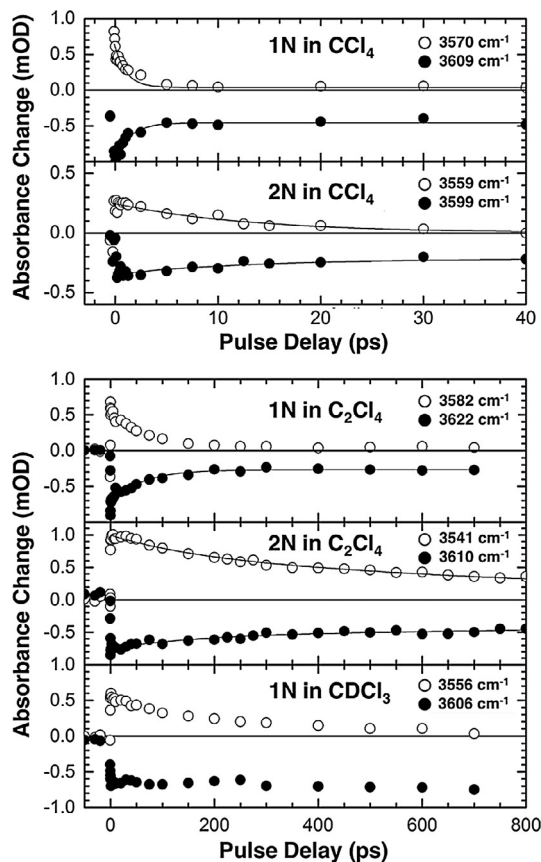


Fig. 4. Transient kinetics of the O–H stretching marker mode, as recorded at frequency positions of the S_0 - and S_1 -states, for 1N and 2N. Note the distinct difference in time scales when comparing CCl_4 with C_2Cl_4 or CDCl_3 solvents. Multi-exponential fits are shown as solid lines (see Table 1 for fitting results). The transient kinetics for 2N in CDCl_3 is very similar to the corresponding kinetics of 1N in CDCl_3 , almost identical within the instrument response resolution.

1N we observe $Y_F(\text{halocarbon})/Y_F(\text{cyclohexane}) = 6 \cdot 10^{-4}$, 0.02, and 0.07 and for 2N we find $Y_F(\text{halocarbon})/Y_F(\text{cyclohexane}) = 3 \cdot 10^{-3}$, 0.17, and 0.18 for CCl_4 , C_2Cl_4 and CDCl_3 , respectively. In addition to that we observe extremely large (partial) ground state recovery rates, with components as fast as the initial electronic excited state decay rates. This is highly surprising because the charge recombination is highly exergonic (more than 3.5 eV). According to Marcus theory (even the semi-classical one), charge recombination should be deeply in the inverted region and therefore slow. This has also been found in previous studies. It suggests that more degrees of freedom are strongly coupled to the reaction coordinate [18, 40–42]. This intriguing finding is currently being investigated with QM/MM calculations, and will be reported on in a future publication. In concluding this section, we note that similar ultrafast relaxation dynamics has been measured for electron donor-acceptor reaction pairs, either as complexes in solution, or between photoexcited donor or acceptor molecules reacting with the solvent [13–18].

4. Theoretical methodology

4.1. Semiclassical Marcus and transition state theories

The multi-exponential decay measured with TCSPC and transient UV/IR experiments (Figs. 2–4) are attributed to electronic de-excitation through multiple pathways, involving both direct ET from the excited naphthol to the halocarbon solvent and ET cou-

pled to *cis-trans* rotamer isomerization of the OH group relative to the aromatic ring (Scheme 1). Marcus theory of electron transfer (Eq. (1), Fig. 5) has become a standard tool for modeling and estimation of ET rates k_{ET} , as determined by the electronic couplings H_{AD} between the electron acceptor and donor parts, the reorganization energy λ estimated as the average of λ_1 and λ_2 as described below (Eq. (2)), the temperature T , and the reaction free energy change ΔG^0 . From the ground and excited state energy manifolds (schematically shown in Fig. 5), we calculate these parameters using DFT and TD-DFT and we obtain the time for de-excitation due to ET as determined by the inverse of the rates estimated with Marcus theory. Note that the reactant (red) and product (black) parabolas have been shown with different curvatures as the calculated values of λ_1 and λ_2 are slightly different. However, to use the Marcus expression (Eq. (1)), an average curvature has been assumed.

Rates of isomerization are obtained from the usual Eyring equation (Eq. (3)), potential energy barriers obtained from a C–C–O–H dihedral scan (Fig. S1 and Table S1).

$$k_{\text{ET}} = \frac{2\pi |H_{\text{AD}}|^2}{\hbar \sqrt{4\pi\lambda k_{\text{B}}T}} \exp\left(-\frac{(\Delta G^0 + \lambda)^2}{4\lambda k_{\text{B}}T}\right) \quad (1)$$

$$\lambda = \frac{\lambda_1 + \lambda_2}{2} \quad (2)$$

$$k_{\text{cis} \rightarrow \text{trans} \text{ or } \text{trans} \rightarrow \text{cis}} = \frac{k_{\text{B}}T}{\hbar} \exp\left(-\frac{\Delta G^\ddagger}{RT}\right) \quad (3)$$

4.2. Computational methods

Reorganization energies, λ , were computed using the B3LYP functional with the 6-31+G(d,p) basis set as implemented in Gaussian 09 D.01 [43] software. The free energies of the optimized naphthol and CCl_4 structures were obtained by using the SMD solvation model [44] and the ‘ultrafine’ integration grid, corrected for finite distance due to the first solvation shell as described in the SI. The reorganization energies λ were computed as described by Eq. (2) as the averages of reorganization energies obtained along the

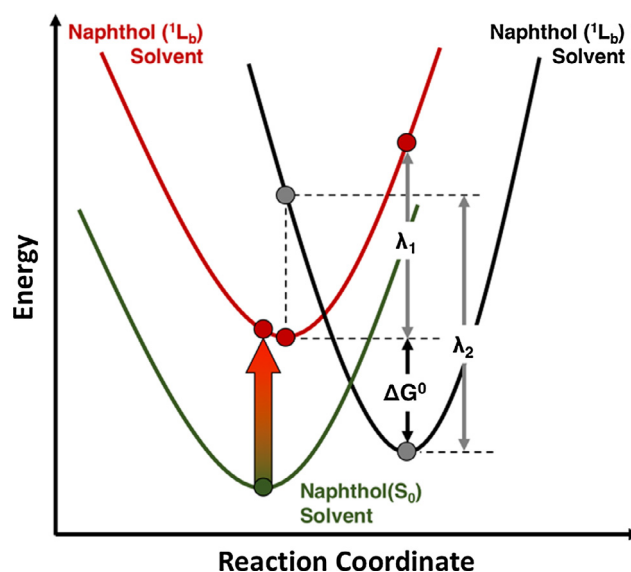


Fig. 5. Schematic energy diagram of the naphthol-halocarbon complex, as approximated by Marcus ET theory.

excited state naphthol + CCl₄ surface (the energy at the minimum subtracted from that at the geometry of the charge transfer state) λ_1 , and the reorganization energy along the charge transfer surface (the energy at the minimum subtracted from that at the geometry of the excited state) λ_2 .

Similarly, vertical (frozen ground state geometry) and adiabatic (relaxed excited state geometry) excitation energies and potential energy surfaces (PES) were calculated using time-dependent DFT (TD-DFT) using the naphthol fragment [45]. The OH rotational free energy barriers, ΔG^\ddagger were estimated from the energies of relaxed conformation obtained by scanning the dihedral angle defining the orientation of OH relative to the aromatic ring.

Free energy changes due to electron transfer, ΔG^0 (Fig. 5), were computed by using constrained DFT [46], at the same level of theory, within the CPCM solvation model, as implemented in the Q-Chem 4.3 program [47]. The naphthol molecule was treated as the donor and the solvent molecule as the acceptor part for the complex in its lowest energy configuration. Both the ground state and the charge transfer state calculations included a damped empirical dispersion term ($f(R) = C/R^6$) from Grimme [48] as well as a Van der Waals scaling factor of 1.35, as found to be useful in our previous work [27]. The free energy of electron transfer is then obtained as the difference between the charge transfer energy and the adiabatic excitation energy.

Assuming no significant change in structure of the naphthol-solvent dyad in the excited state, LUMO-LUMO electronic couplings (H_{AD}) were calculated for the optimized models determined by constrained DFT. The B3LYP/TZ2P level (Voronoi integration keyword = 5) of theory with the COSMO dielectric model was used in the ADF package [49,50] to calculate the couplings.

4.3. Kinetic model

To model the multi-exponential excited state relaxation, we built a kinetic model based on the rates for electron transfer cis and trans (1N and 2N) conformers, $k_{cis \rightarrow CS}$ and $k_{trans \rightarrow CS}$, respectively, as they form charge separated (CS) states by ET to the solvent, and the isomerization rate constants associated with cis-trans interconversion, $k_{cis \rightarrow trans}$ and $k_{trans \rightarrow cis}$ due to the rotational motion of OH relative to the aromatic ring. The corresponding kinetic equations are given in the SI (Eqs. S1–S5). The OH rotational free energy difference between these conformers, ΔG , gives Boltz-

mann populations in the ground state that are 93% and 29% in favor of the *trans*-rotamer for 1N and 2N respectively [35]. The overall decay constants are then obtained by fitting the net population decay to a single exponential decay model, consistently with the treatment of experimental data (Fig. S5). We note here that the kinetics of the 1N and 2N in CCl₄ is predominantly governed by the individual CS decay channels of the two rotamers. For C₂Cl₄ and CHCl₃ as a solvent, where the respective CS of the two rotamers are significantly slower, a competition between CS and rotamer exchange plays a major role. More details will be provided in a future publication from our QM/MM calculations on 1N and 2N in these other solvents.

5. Theoretical results

Fig. 6 shows relaxed configurations of 1N- and 2N-halocarbon complexes, with favorable overlaps of LUMO's to facilitate ET after photoexcitation of the 1N and 2N moieties in the weakly coupled ET donor-acceptor (D-A) systems. The two lowest-lying electronic states of the naphthols were identified as the ¹L_a and ¹L_b states, according to their corresponding electronic symmetries. In the absence of the OH functional group, the transition dipole moments of the ¹L_a and ¹L_b states are polarized perpendicularly to each other. The ¹L_a transition dipole moment is oriented through the short-axis along the central C–C bond connecting the two aromatic rings, while the forbidden ¹L_b transition dipole points along the long through-bond axis [35]. The presence of the OH-group at the 1- or 2- position for 1N and 2N, respectively, breaks the symmetry of an otherwise symmetric molecule (naphthalene) and partially mixes the two electronic states, changing the relative energy spacing and magnitudes of the transition dipole moments. While the ¹L_a state is optically strongly active (as prepared by the TCSPC measurements), rapid internal conversion leads to population of the ¹L_b state. As such, ET rates from the ¹L_b state were computed (as actually prepared in the ultrafast UV/IR experiments), using the calculated DFT parameters summarized in Table 2. These Marcus theory rates were fed into the kinetic model as described above to get overall decay constants more directly comparable to experiment. Additional relaxed configurations were also calculated as shown in Fig. S4 and their rates are given in Table S2. As noted in Fig. 1(a,b), the fluorescence spectra of the S₀ ← ¹L_b (S₁) electronic transition is red shifted by 1700–2000 cm⁻¹ from the absorption

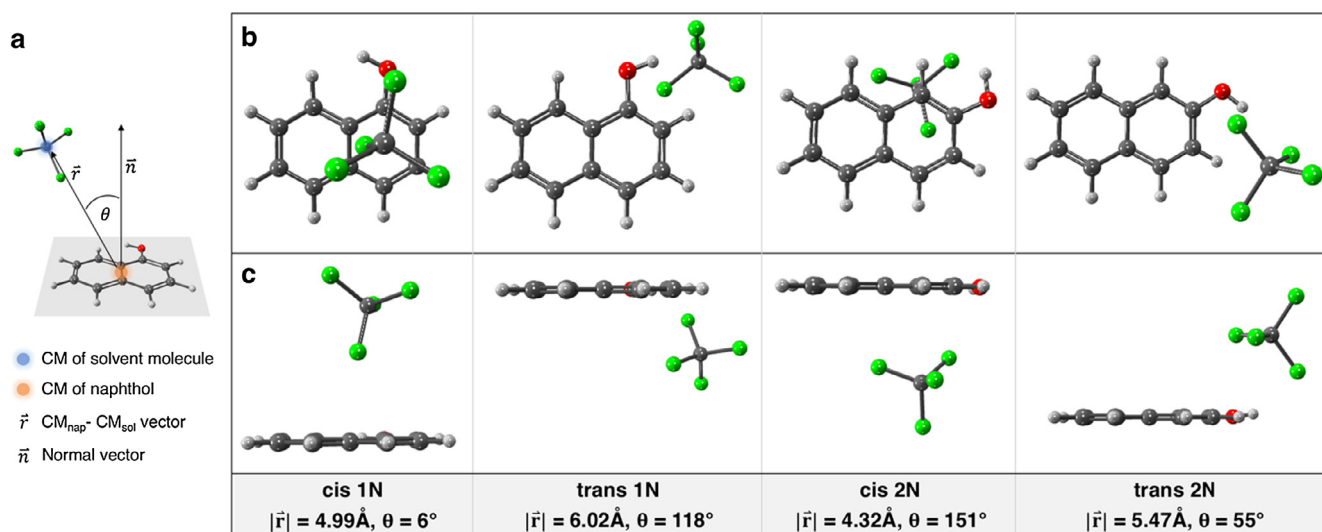


Fig. 6. (a) Schematic figure showing the position parameters ($|\vec{r}| = \text{CM}_{\text{naph}} - \text{CM}_{\text{sol}}$ distance, $\theta =$ Angle between normal to the plane of the naphthol (\vec{n}) and \vec{r}). (b) Top and (c) side views of 1N- and 2N-CCl₄ complexes in their relaxed configurations.

Table 2

Marcus parameters for 1N and 2N in CCl₄, including the ET time for the minimum energy structure ($t_{\min E}$), the ET time according to a single exponential fit of the kinetic model results ($t_{\min E, \text{fit}}$), the experimental times ($t_{\text{Experiment}}$), and the interconversion between cis and trans isomers ($t_{\text{Conv.}}$).

	ΔG [eV]	$S_0 \rightarrow {}^1L_b$ (vertical) [eV]	$S_0 \rightarrow {}^1L_b$ (adiabatic) [eV]	λ_{tot} [eV]	$ H_{\text{AD}} $ [eV]	$t_{\min E}$ [ps]	$t_{\min E, \text{fit}}$ [ps]	$t_{\text{Experiment}}$ [ps]	$t_{\text{Conv.}}$ [ps]
cis 1N	-0.60	4.28	4.18	1.29	0.029	2.75	3.2	1.4	4.3
trans 1N	-0.55	4.47	4.20	1.28	0.030	3.21			49
cis 2N	-0.29	4.32	4.34	1.26	0.083	12.63	13.1	13	57
trans 2N	-0.30	4.46	4.33	1.29	0.090	14.40			26

spectra which can be attributed to stabilization of the S_1 state in conjunction with destabilization of the S_0 state upon excited state relaxation. The stabilization of the S_1 state shifts the geometry of the chromophore closer to the geometry of the product, decreasing both ΔG^0 and λ and leading to partial cancellation of the effects of relaxation on the charge transfer rates.

6. Discussion

6.1. Comparison of electron transfer rates with experiment

Table 2 shows that the theoretical decay constants, both as directly from Marcus theory and as resulting from the kinetic model as shown in Fig. S5, for the configurations in Fig. 6 are in reasonable agreement with experiment. While pulse-width limitations prevent us from experimentally distinguishing the dynamics of individual conformers, rotamer exchange is inferred from the overall reaction kinetics studied through the kinetic model. The effects of possible rotamer exchange is less pronounced in CCl₄ due to ultrafast charge separation times. However, this is not the case for C₂Cl₄ and CHCl₃, where the competition between respective CS and rotamer exchange is a major part of the overall reaction kinetics. Consistent with experimental observations, the calculations show that 2N decays more slowly than 1N for both *cis* and *trans* configurations. These trends are also consistent with differences in the interactions between the halocarbon and the aromatic ring of 1N and 2N in their closest contact configurations (Fig. 6). Both *cis* isomers stabilize close-contact configurations (with the halocarbon at 4–5 Å from the ring at on-top configurations with $\theta \approx 0$ or 180°), while the *trans* isomers stabilize contact configurations of the halocarbon farther away (at 5–6 Å from the ring with $\theta \approx 90^\circ$). The *trans* isomers thus exhibit longer decay times due to the weaker contact with the π -electronic system, because they have their OH groups pointing toward the less sterically crowded portion of the ring. Thus, the orientation of the OH substituent group modulates the relative arrangement of the D-A pair in their most strongly interacting configuration.

We note that configurations of the D-A pair that gave less agreement with experiment (Fig. S4 and Table S2) feature D-A contact from the side of the ring, often giving rates that are much faster or slower. These configurations would be statistically less likely than the configurations in Fig. 6, which feature direct Cl-naphthol contact.

7. Conclusions

In conclusion, we observe ultrafast de-excitation pathways in the picosecond time scale for the electronically excited photoacids 1-naphthol and 2-naphthol, ascribe to electron transfer to the halogenated alkane solvent followed by back electron transfer resulting in ground state recovery. The analysis of the mechanism based on Marcus theory and a kinetic model suggests that the observed decay times and trends in de-excitation rates of 1-naphthol and 2-naphthol originate from differences in interactions between

the two halocarbons and the π -electronic structure of the naphthol.

Author contributions

The manuscript was written through contributions of all authors. All authors have given approval to the final version of the manuscript.

Acknowledgment

V.S.B. acknowledges support from the National Science Foundation (NSF) Grant CHE 1213742 and supercomputer time from NERSC and the Yale University Faculty of Arts and Sciences High Performance Computing Center partially funded by the NSF Grant CNS 08-21132. B.R. acknowledges support from the National Science Foundation Graduate Research Fellowship under Grant No. DGE-1122492. This work used the Extreme Science and Engineering Discovery Environment (XSEDE), which is supported by National Science Foundation grant number ACI-1053575. E.T.J.N. acknowledges support from the German Science Foundation (Project Nr. DFG - NI 492/11-1). The authors would like to thank Marius Frank, Dr. Svante Hedström, and Dr. Heidi Hendrickson for helpful discussions on Marcus theory and constrained DFT optimization.

Appendix A. Supplementary material

Computed C–C–O–H dihedral scans, details of MD and resulting radial distribution functions, information of the identification of excited state transitions, transition dipole moments, conversion rates between isomers, additional configurations and ET rates, kinetic model plot, derivation of the kinetic model, and minimum energy coordinates in the form of xyz files. Supplementary data associated with this article can be found, in the online version, at <http://dx.doi.org/10.1016/j.cplett.2017.03.080>.

References

- [1] N. Mataga, H. Chosrowjan, S. Taniguchi, J. Photochem. Photobiol., C 6 (2005) 37.
- [2] J. Jortner, M. Bixon, Advances in Chemical Physics: Electron Transfer-from Isolated Molecules to Biomolecules, Wiley, 1999.
- [3] A.H. Zewail, Science 242 (1988) 1645.
- [4] P. Cheng, D. Zhong, A.H. Zewail, J. Chem. Phys. 103 (1995) 5153.
- [5] T. Fiebig, C. Wan, S.O. Kelley, J.K. Barton, A.H. Zewail, P. Natl. Acad. Sci. USA 96 (1999) 1187.
- [6] K. Wynne, G.D. Reid, R.M. Hochstrasser, J. Chem. Phys. 105 (1996) 2287.
- [7] Y. Keitaro, T. Keisuke, N. Yutaka, Bull. Chem. Soc. Jpn. 68 (1995) 696.
- [8] H. Shirota, H. Pal, K. Tominaga, K. Yoshihara, J. Phys. Chem. A 102 (1998) 3089.
- [9] E.W. Castner, D. Kennedy, R.J. Cave, J. Phys. Chem. A 104 (2000) 2869.
- [10] Q.-H. Xu, G.D. Scholes, M. Yang, G.R. Fleming, J. Phys. Chem. A 103 (1999) 10348.
- [11] P.F. Barbara, T.J. Meyer, M.A. Ratner, J. Phys. Chem. 100 (1996) 13148.
- [12] R.A. Marcus, N. Sutin, Biochem. Biophys. Acta. 811 (1985) 265.
- [13] A. Rosspeintner, B. Lang, E. Vauthey, Annu. Rev. Phys. Chem. 64 (2013) 247.
- [14] M. Delor, P.A. Scattergood, I.V. Sazanovich, A.W. Parker, G.M. Greetham, A.J. Meijer, M. Towrie, J.A. Weinstein, Science 346 (2014) 1492.
- [15] M. Koch, A. Rosspeintner, K. Adamczyk, B. Lang, J. Dreyer, E.T.J. Nibbering, E. Vauthey, J. Am. Chem. Soc. 135 (2013) 9843.

- [16] O.F. Mohammed, K. Adamczyk, N. Banerji, J. Dreyer, B. Lang, E.T.J. Nibbering, E. Vauthey, *Angew. Chem. Int. Ed.* 47 (2008) 9044.
- [17] F. Provencher, N. Bérubé, A.W. Parker, G.M. Greetham, M. Towrie, C. Hellmann, M. Côté, N. Stingelin, C. Silva, S.C. Hayes, *Nat. Commun.* 5 (2014).
- [18] H.N. Ghosh, K. Adamczyk, S. Verma, J. Dreyer, E.T.J. Nibbering, *Chem. Eur. J.* 18 (2012) 4930.
- [19] L. Genosar, B. Cohen, D. Huppert, *J. Phys. Chem. A* 104 (2000) 6689.
- [20] O.F. Mohammed, D. Pines, J. Dreyer, E. Pines, E.T.J. Nibbering, *Science* 310 (2005) 83.
- [21] K. Adamczyk, M. Prémont-Schwarz, D. Pines, E. Pines, E.T.J. Nibbering, *Science* 326 (2009) 1690.
- [22] E. Pines, D. Huppert, *J. Chem. Phys.* 84 (1986) 3576.
- [23] D. Pines, E.T.J. Nibbering, E. Pines, *Isr. J. Chem.* 55 (2015) 1240.
- [24] E. Pines, B.-Z. Magnes, M.J. Lang, G.R. Fleming, *Chem. Phys. Lett.* 281 (1997) 413.
- [25] G. Granucci, J.T. Hynes, P. Millie, T.-H. Tran-Thi, *J. Am. Chem. Soc.* 122 (2000) 12243.
- [26] N. Agmon, W. Rettig, C. Groth, *J. Am. Chem. Soc.* 124 (2002) 1089.
- [27] B.T. Psciuk, M. Prémont-Schwarz, B. Koeppel, S. Keinan, D. Xiao, E.T.J. Nibbering, V.S. Batista, *J. Phys. Chem. A* 119 (2015) 4800.
- [28] P.K. Behera, A.K. Mishra, *J. Photochem. Photobiol., A* 71 (1993) 115.
- [29] P.K. Behera, T. Mukherjee, A.K. Mishra, *J. Lumin.* 65 (1995) 131.
- [30] P.K. Behera, T. Mukherjee, A.K. Mishra, *J. Lumin.* 65 (1995) 137.
- [31] M.V. Encinas, M.A. Rubio, E.A. Lissi, *J. Photochem.* 18 (1982) 137.
- [32] C. Lewis, W.R. Ware, *Chem. Phys. Lett.* 15 (1972) 290.
- [33] D. Saperstein, E. Levin, *J. Chem. Phys.* 62 (1975) 3560.
- [34] M. Prémont-Schwarz, D. Xiao, V.S. Batista, E.T.J. Nibbering, *J. Phys. Chem. A* 115 (2011) 10511.
- [35] D. Xiao, M. Prémont-Schwarz, E.T.J. Nibbering, V.S. Batista, *J. Phys. Chem. A* 116 (2011) 2775.
- [36] S. Chaudhuri, S. Hedström, D.D. Méndez-Hernández, H.P. Hendrickson, K.A. Jung, J. Ho, V.S. Batista, 2017, submitted for publication.
- [37] R. Simkovitch, D. Pines, N. Agmon, E. Pines, D. Huppert, *J. Phys. Chem. B* 120 (2016) 12615.
- [38] F. Messina, M. Prémont-Schwarz, O. Braem, D. Xiao, V.S. Batista, E.T.J. Nibbering, M. Chergui, *Angew. Chem. Int. Ed.* 52 (2013) 6871.
- [39] M. Prémont-Schwarz, T. Barak, D. Pines, E.T.J. Nibbering, E. Pines, *J. Phys. Chem. B* 117 (2013) 4594.
- [40] E. Buhks, M. Bixon, J. Jortner, *G. Navon, J. Phys. Chem.* 85 (1981) 3759.
- [41] T. Guarr, E. Buhks, G. McLendon, *J. Am. Chem. Soc.* 105 (1983) 3763.
- [42] P. Siders, R. Marcus, *J. Am. Chem. Soc.* 103 (1981) 4.
- [43] M.J.T. Frisch, G.W. Trucks, H.B. Schlegel, G.E. Scuseria, M.A. Robb, J.R. Cheeseman, G. Scalmani, V. Barone, B. Mennucci, G.A. Petersson, H. Nakatsuji, M. Caricato, X. Li, H.P. Hratchian, A.F. Izmaylov, J. Bloino, G. Zheng, J.L. Sonnenberg, M. Hada, M. Ehara, K. Toyota, R. Fukuda, J. Hasegawa, M. Ishida, T. Nakajima, Y. Honda, O. Kitao, H. Nakai, T. Vreven, J.A. Montgomery, J.E. Peralta Jr., F. Ogliaro, M. Bearpark, J.J. Heyd, E. Brothers, K. N. Kudin, V.N. Staroverov, R. Kobayashi, J. Normand, K. Raghavachari, A. Rendell, J.C. Burant, S.S. Iyengar, J. Tomasi, M. Cossi, N. Rega, N.J. Millam, M. Klene, J.E. Knox, J.B. Cross, V. Bakken, C. Adamo, J. Jaramillo, R. Gomperts, R.E. Stratmann, O. Yazyev, A.J. Austin, R. Cammi, C. Pomelli, J.W. Ochterski, R.L. Martin, K. Morokuma, V.G. Zakrzewski, G.A. Voth, P. Salvador, J.J. Dannenberg, S. Dapprich, A.D. Daniels, Ö. Farkas, J.B. Foresman, J.V. Ortiz, J. Cioslowski, D.J. Fox, *Gaussian 09 Revision D.01*. Gaussian Inc, Wallingford CT, 2009.
- [44] A.V. Marenich, C.J. Cramer, D.G. Truhlar, *J. Phys. Chem. B* 113 (2009) 6378.
- [45] G. Scalmani, M.J. Frisch, B. Mennucci, J. Tomasi, R. Cammi, V. Barone, *J. Chem. Phys.* 124 (2006) 094107.
- [46] Q. Wu, T. Van Voorhis, *J. Phys. Chem. A* 110 (2006) 9212.
- [47] Y. Shao, Z. Gan, E. Epifanovsky, A.T. Gilbert, M. Wormit, J. Kussmann, A.W. Lange, A. Behn, J. Deng, X. Feng, *Mol. Phys.* 113 (2015) 184.
- [48] S. Grimme, *J. Comput. Chem.* 27 (2006) 1787.
- [49] G. te Velde, E.J. Baerends, *J. Comput. Phys.* 99 (1992) 84.
- [50] G. te Velde, F.M. Bickelhaupt, E.J. Baerends, C. Fonseca Guerra, S.J. van Gisbergen, J.G. Snijders, T. Ziegler, *J. Comput. Chem.* 22 (2001) 931.